Automated Detection and Characterization of Surface Restructuring Events in Bimetallic Catalysts

Jin Soo Lim,[*,†] Nicola Molinari,[‡] Kaining Duanmu,[¶] Philippe Sautet,[¶,§] and Boris Kozinsky[*,‡,‖]

†*Department of Chemistry and Chemical Biology, Harvard University, Cambridge, MA 02138, USA*

‡*John A. Paulson School of Engineering and Applied Sciences, Harvard University, Cambridge, MA 02138, USA*

¶*Department of Chemical and Biomolecular Engineering, University of California, Los Angeles, California 90095, USA*

§*Department of Chemistry and Biochemistry, University of California, Los Angeles, California 90095, USA*

‖*Robert Bosch LLC, Research and Technology Center, Cambridge, MA 02142, USA*

E-mail: limjs@g.harvard.edu; bkoz@seas.harvard.edu

Abstract

Surface restructuring in bimetallic systems has recently been shown to play a crucial role in heterogeneous catalysis. In particular, the segregation in binary alloys can be reversed in the presence of strongly bound adsorbates. Mechanistic characterization of such restructuring phenomena at the atomic level remains scarce and challenging due to the large configurational space that must be explored. To this end, we propose an

automated method to discover elementary surface restructuring processes in an unbiased fashion, using Pd/Ag as an example. We employ high-temperature classical molecular dynamics (MD) to rapidly detect restructuring events, isolate them, and optimize using density functional theory (DFT). In addition to confirming the known exchange descent mechanism, our systematic approach has revealed three new predominant classes of events at step edges of close-packed surfaces that have not been considered before: (1) vacancy insertion; (2) direct exchange; (3) interlayer exchange. The discovered events enable us to construct the complete set of mechanistic pathways by which Pd is incorporated into the Ag host in vacuum at the single-atom limit. These atomistic insights provide a step toward systematic understanding and engineering of surface segregation dynamics in bimetallic catalysts.

Introduction

Fundamental knowledge of atomic surface structure lies central to heterogeneous catalysis. The electronic and geometric characteristics of the surface active site influence the thermodynamics and kinetics of the underlying microscopic mechanism of a chemical reaction, which in turn determine the activity and selectivity of the catalyst at the macroscopic level.[1] Total energy calculations based on density functional theory (DFT) allow one to thoroughly map out different reaction pathways on a given model surface,[2] highlighting the crucial role of computational methods in advancing rational catalyst design principles.[3,4] However, this approach is inherently static, meaning it assumes a certain surface structure and reaction mechanism. This limitation requires one to perform multiple computations in order to discover the most relevant sets of structures and mechanisms, which can quickly become computationally expensive and intractable if attempted without some prior knowledge of the system.

One of the most challenging issues to tackle in this regard is the surface restructuring phenomenon. Increasing evidence indicates that catalytic surfaces are rarely static at most

reaction temperatures of interest (room temperature and above). In fact, surface composition and morphology can further be altered in the presence of strongly bound adsorbates, which means that the surface ensemble distribution *in operando* can differ widely from that of the as-synthesized catalyst.[1,5–8] This dynamic nature of the catalyst poses an additional challenge for static *ab initio* methods due to the large configurational space intrinsic to such restructuring processes. In the computational literature, several methods in addition to DFT[6,9–13] have been employed successfully to study surface restructuring *in vacuo*, most prominently classical molecular dynamics (MD),[14–16] kinetic Monte Carlo (KMC),[17–19] Monte Carlo (MC),[20–22] and genetic algorithm,[23,24] most frequently using embedded-atom method (EAM) potential or second-moment approximation of tight-binding (SMA-TB) potential. Compared to DFT, these methods have the advantage of computational speed and scalability, as well as more efficient exploration of configurational space, but at the cost of using interatomic potentials with lower accuracy and transferability.

Historically, surface restructuring of late transition metals can be classified into three main categories: (1) surface relaxation[25] involving local displacements around the atomic sites; (2) surface reconstruction[14,26–28] and adatom diffusion in epitaxial island growth[29] involving changes in the atomic sites within the surface layer; (3) surface segregation in alloys[30,31] involving changes in the atomic sites across surface and subsurface layers. In surfaces, reduced coordination number results in reduced d-band width and increased tensile stress.[25] All restructuring processes are driven by the tendency to lower the surface free energy. Bimetallic systems, of particular interest for selective hydrogenation, possess additional complexity due to elemental variations in the surface energy. Elements with fuller d-shell have lower surface energy and segregate to the surface at equilibrium in vacuum. A method of achieving activity-selectivity balance for hydrogenation has been to alloy highly active Group 10 metals (Ni, Pd, Pt) with noble Group 11 metals (Cu, Ag, Au), which demonstrate low H_2 activation due to their full d-shell, or *vice versa*.[32–37] In these systems, Group 11 metals segregate to the surface after annealing, while Group 10 metals migrate to the

subsurface, forming core@shell nanostructures.[22] The thermodynamics of such segregation phenomenon has been studied extensively in the computational literature as a function of size mismatch, miscibility, composition, cluster size, cluster shape, and temperature, especially for Pd-doped Group 11 systems: Pd@Cu;[19,31,38–44] Pd@Ag;[44–69] Pd@Au.[45,62,68,70–85]

Thermodynamically, surface segregation can be understood within the framework of the quasi-chemical approximation,[86] where surface and subsurface species are modeled to be in a state of chemical equilibrium. The energetic contributions consist of four components: (1) surface energy; (2) strain energy; (3) alloying energy; (4) adsorption energy. The first three components have been described as "the three effects' rule",[31] whereas the last component has been termed "the chemical pump effect"[87,88] due to the ability of adsorbates to reverse the segregation. Numerous studies have employed DFT to investigate adsorbate-induced reverse segregation in Pd-doped Group 11 systems, where Pd is now stabilized on the surface by adsorbates such as CO,[5,13,89–109] O,[5,105,110–116] and H.[97,102,105,108,117–120] In Pd/Ag, for example, CO provides a stronger driving force for Pd segregation compared to H,[105] whereas O can exhibit complex coverage-dependent formation of surface oxide phases.[5,121] These observations suggest CO and O pretreatment as a promising way of activating or deactivating bimetallic catalysts.[5]

Almost all of the aforementioned DFT studies employ a static approach, using flat model terraces to calculate segregation energy, defined as the change in energy as Pd goes from subsurface to surface. However, segregation energy is a thermodynamic quantity and as such lacks any mechanistic or kinetic information. For example, the actual energy barrier for Pd-Au exchange is expected to be high at terraces[101] and lower at less coordinated sites such as edges and corners.[92] To our best knowledge, only three studies by An & Kim *et al.*[92,101] and Yang *et al.*[89] have investigated transition state pathway for CO-induced Pd segregation in Au. However, these studies assume simple pathways that are specific to terraces and corners, precluding possible concerted motions involving step edges. Furthermore, a KMC study by Cheng *et al.*[19] has shown that Pd/Cu segregation completes within 900 s at 500 K *in vacuo*,

but the corresponding time scale under reaction conditions remains unclear.

These mechanistic and kinetic information are important for the following reason. Reverse segregation plays a crucial role in catalytic activity by allowing the more active metal to be present on the surface. However, adsorbates can also promote aggregation of the active metal atoms,[6,13,94,104,122,123] which can facilitate unwanted side reactions such as coupling.[2] Therefore, mechanistic understanding and control of reverse segregation are needed in order to engineer surface ensemble distributions for optimal activity-selectivity balance.[6,122]

To this end, we propose an automated method to map out elementary surface restructuring processes in an unbiased fashion, using Pd/Ag as an example. Our approach combines molecular dynamics and static *ab initio* calculations in order to overcome the limitations of

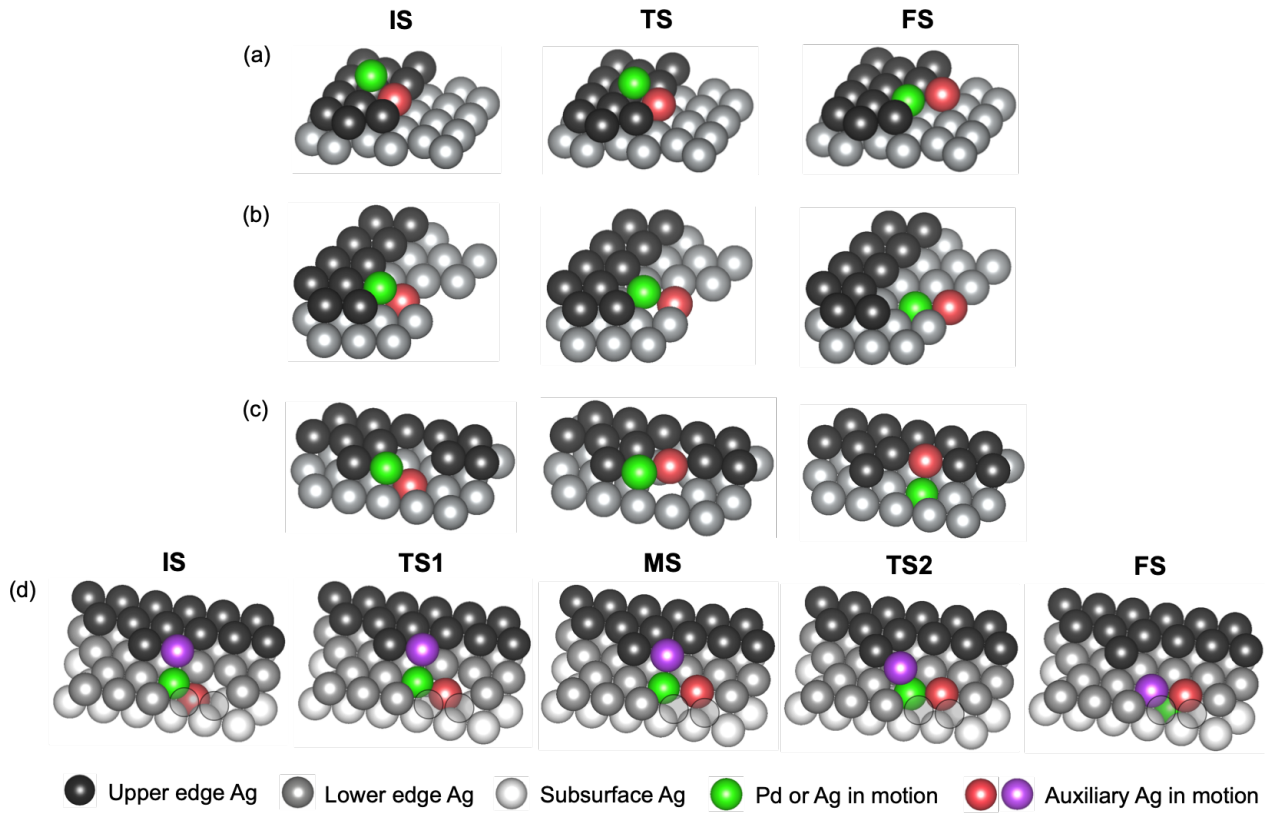

Figure 1: Four main types of restructuring events at step edges of close-packed surfaces, as discovered from classical MD. The structures shown (IS = initial state; TS = transition state; MS = metastable state; FS = final state) are fully optimized using DFT, with forward energy barriers lower than 0.60 eV: (a) exchange descent; (b) vacancy insertion; (c) direct exchange; (d) interlayer exchange.

conventional transition state modeling methods. We utilize MD simulations at an elevated temperature using an EAM potential for fast simulation and detection of restructuring events *in vacuo*, after which the events are isolated and their energetics characterized more accurately using DFT. Our method has revealed four main classes of concerted events at step edges of close-packed surfaces (Fig. 1). In turn, realistic mechanisms can be constructed for Pd incorporation into the Ag host at the single-atom limit, opening up a pathway toward systematic understanding and engineering of surface segregation in bimetallic catalysts.

Computational Details

Density functional theory

We perform density functional theory (DFT) calculations[124] using plane-wave basis sets[125] and the projector augmented-wave (PAW) method[126,127] as implemented in the Vienna *Ab Initio* Simulation Package (VASP).[128] The plane-wave kinetic energy cutoff is set at 450 eV. The Methfessel-Paxton smearing scheme[129] is employed with a broadening value of 0.2 eV. The Brillouin zone is sampled using Γ-centered k-point grids. All initial and final state candidates are optimized via ionic relaxation, where the total energy and forces are converged to 10^{-5} eV and 0.02 eV/Å, respectively. Transition state candidates are fully optimized to first-order saddle points via the dimer method[130] as implemented in the VASP Transition State Tools (VTST),[131] this time converging the total energy and forces to 10^{-7} eV and 0.01 eV/Å, respectively. For representative restructuring events, we confirm that the normal modes of all transition states contain only one imaginary frequency (See Sec. 9, Supporting Information). The Hessian matrix is calculated within the harmonic approximation using central differences of 0.01 Å, at the same level of accuracy as the dimer method.

Lattice constants of bulk face-centered cubic (FCC) Ag and Pd are optimized according to the third-order Birch-Murnaghan equation of state,[132,133] using a 19×19×19 k-point grid. We maintain the lattice constant of pure Ag for all Pd-doped Ag systems, as we only consider

Table 1: Computational set-up of Ag slab models considered for surface restructuring processes.

Facet	Features	Unit cell	Number of layers	k-point grid
(111)	Close-packed terrace (CPT)	4×4	6 (bottom 1 fixed)	5×5×1
(533)	4-row CPT with A-step edge	4×4	4 (bottom 1 fixed)	5×5×1
(221)	4-row CPT with B-step edge	8×4	4 (bottom 1 fixed)	3×5×1

Pd dopants as isolated atoms in the dilute limit ($<$ 2 at. %). All slab models are spaced by 16 Å of vacuum along the direction normal to the surface in order to avoid spurious interactions between adjacent unit cells. The bottom-most layer is fixed at its bulk position to prevent it from acting as a surface. Table 1 describes the computational set-up of the slab models of close-packed Ag surface considered in our study. Two possible step terminations exist for a close-packed surface (See Table 2): A-step with (100)-type termination; B-step with (111)-type termination.

We test different pair-wise vdW corrections[134–137] and nonlocal self-consistent vdW functionals[138–142] for Ag and Pd bulk properties (See Sec. 1, Supporting Information). We find that vdW density functional (vdW-DF) correlation[138] with optPBE exchange (PBE[143] exchange optimized for vdW-DF),[140] hereby referred to as optPBE-vdW, gives cohesive energy of 2.71 and 3.84 eV for Ag and Pd, respectively, in good agreement with the experimental benchmark of 2.97 eV and 3.92 eV.[142] In addition, we obtain solvation energy of -34 meV for a single Pd atom in a pure Ag matrix, consistent with a small negative value of -17 meV reported for experimental mixing enthalpy at 20 at. % Pd measured at 600 K.[144] As such, all DFT calculations in this study are performed using optPBE-vdW, unless stated otherwise.

Molecular dynamics

We perform molecular dynamics (MD) simulations using the Large-scale Atomic/Molecular Massively Parallel Simulator (LAMMPS).[145] We use Pd-Ag-H ternary embedded-atom method (EAM) potential developed by Hale *et al.*[146] To test the suitability of the potential, we perform several static calculations at 0 K including ionic relaxation with forces converged to

0.001 eV/Å, using our DFT energetics as a benchmark (See Sec. 4, Supporting Information). We employ periodic boundary condition in the xy-direction parallel to the plane containing the surface. First, because the EAM potential reverses the stability hierarchy of different H adsorption sites on Ag from that obtained by DFT, we henceforth preclude H from all MD simulations. Second, the EAM potential is in qualitative agreement with DFT on the stability of Pd dopant in Ag: Pd prefers to reside at subsurface sites *in vacuo*.

Given this qualitative agreement on Pd/Ag energetics, we next test adatom diffusion dynamics on close-packed terrace to validate the suitability of the potential for describing basic surface atomic motions. The bottom-most layer is frozen at 0 K (velocities and forces set to zero). A velocity-Verlet integrator with a time step of $\delta t = 5.0$ fs is used to evolve the equations of motion. Pressure and temperature are enforced on the system with a Nosé-Hoover barostat (1000 $\delta t = 5$ ps coupling) and thermostat (100 $\delta t = 0.5$ ps coupling), respectively.[147–149] All simulations consist of 1 ns equilibration within the isothermal-isobaric (NPT) ensemble, followed by 20 ns production within the canonical (NVT) ensemble.

We construct the Arrhenius plot of adatom self-diffusion on Ag(111) (See Sec. 5, Supporting Information), from which we obtain an activation energy of 88 meV, in good agreement with the corresponding static value of 70 meV, the recent EAM-KMC value of 59 meV,[17] our DFT value of 51 meV, and the experimental values reported in the range of 50-180 meV (See Lü *et al.*[18] and references therein). Our diffusion prefactor of 2.44×10^{12} Å^2/s is also in good agreement with the recent EAM-KMC value of 2.24×10^{12} Å^2/s.[17]

For Pd adatom diffusion on Ag(111), we obtain a static value of 26 meV for the activation energy, in good agreement with our DFT value of 31 meV. We do not construct the corresponding Arrhenius plot because our MD simulations show that Pd easily becomes incorporated into the Ag host above 400 K (See Sec. 5, Supporting Information), in agreement with recent experimental observations of van Spronsen *et al.*[5] To our best knowledge, there are no experimental or computational benchmark available in the literature for Pd/Ag(111) heteroepitaxial adatom diffusion.

Suitable restructuring event trajectories extracted from MD are optimized via the climbing-image nudged elastic band (CI-NEB) method[150,151] as implemented in LAMMPS, where the total forces, given as the sum of the spring force along the chain and the true force orthogonal to the chain, are converged to 0.001 eV/Å.

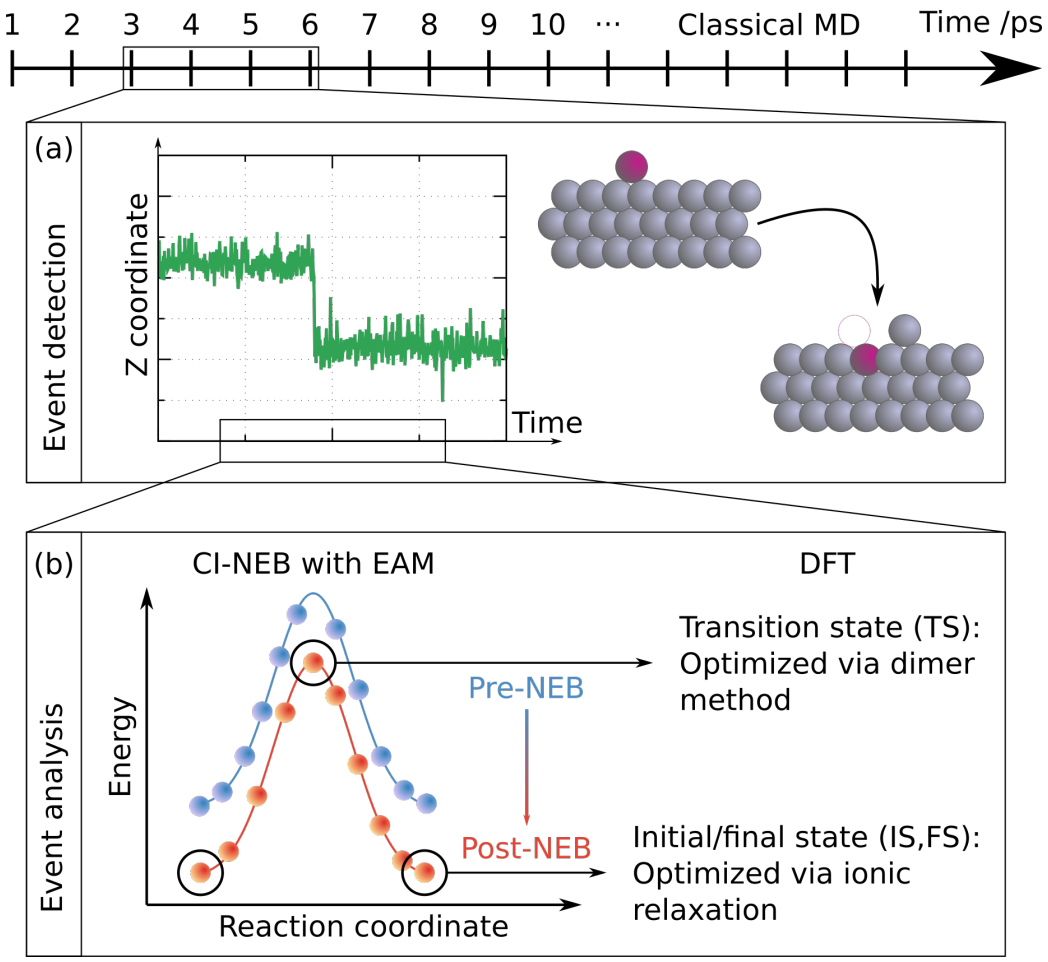

Figure 2: Schematic of the automated restructuring event extraction process. A 20 ns classical MD trajectory is post-processed: (a) An event is detected whenever z-coordinate of any atom changes by more than 80% of the average interlayer distance within 1-2 ps time window. (b) After detection, the corresponding trajectory fragment is further processed through the CI-NEB method to obtain suitable initial, transition, and final state candidates, which are subsequently optimized using DFT.

Restructuring event extraction scheme

Here, we describe our automated restructuring event extraction scheme (Fig. 2) in detail, as well as outline and justify the main underlying assumptions. First, we perform MD simulation using the EAM potential. Based on the validation summarized above, we conclude that the EAM potential is qualitatively reasonable enough to describe the basic atomic diffusion and rearrangement processes in the top 3 surface layers in the absence of adsorbed H.

For our MD simulation, we employ the same unit cell to be used later in DFT optimization (Table 1). There are two reasons for this choice: (1) Using the DFT unit cell eliminates the need to perform a nontrivial "cut out" of a periodic unit cell of suitable size for later DFT analysis. (2) Smaller unit cell prevents multiple restructuring events from happening at the same time and potentially interacting with each other (See Sec. 6, Supporting Information for further justification).

We use pure Ag surfaces to simulate restructuring processes, after which the active atom is substituted with Pd in the DFT optimization. This choice is mainly for convenience and can be justified as follows. (1) Introducing Pd dopant into the MD simulation would require us to track the Pd atom, which can result in missing other restructuring events involving only Ag atoms that the Pd atom in principle could undergo as well. Therefore, the strategy of introducing Pd post-detection allows for a more comprehensive and efficient sampling of the events. The strategy also allows a direct comparison of Ag/Ag versus Pd/Ag energetics for each event. (2) We find that a Pd atom easily becomes incorporated into the Ag host above 400 K and remains in the subsurface thereafter (See Sec. 5, Supporting Information). (3) Introducing Pd dopant in the dilute limit (< 2 at. % in our simulation) is not expected to fundamentally alter the set of possible restructuring events as observed on pure Ag surfaces. A single, isolated Pd atom is expected to impose a relatively small strain in its local Ag environment, based on the small difference ($\approx 4.6\%$) of Pd lattice constant from that of Ag.[142] Furthermore, the electronic effect is also expected to be small, based on the projected

density of states of Pd/Ag(111) single-atom alloy, as reported in a recent DFT study of Thirumalai *et al.*,[152] which consists of a sharp Pd d-band peak having a negligible overlap with the Ag d-band. If the alloy system of interest experiences significant electronic and geometric effect due to large differences between the constituent elements, one can always perform an ensemble of MD simulations with the alloy structure of realistic compositions and track the motion of the active atoms individually.

We test a temperature range of 300-1200 K to determine the optimal temperature at which the simulation produces an adequate number of restructuring events within the total simulation time of 20 ns. We find that an elevated temperature of 1100 K for Ag(111), and 1000 K for Ag(533) and Ag(221), is needed to trigger sufficient amount of interlayer restructuring within the 20 ns period (See Sec. 6, Supporting Information).

We note two important points regarding this thermally accelerated sampling scheme: (1) The simulated melting temperature of bulk FCC Ag using the EAM potential was reported to be 1267 K,[153] with the experimental value of 1235 K.[154] We do not observe any Ag surface pre-melting[155–157] of our close-packed slab models at the chosen simulation temperatures of 1000-1100 K, in agreement with a previous EAM study that also observed no surface pre-melting in Ag(111) up to 1100 K.[158] (2) The set of possible restructuring events is expected to remain nearly invariant across the temperature range considered. In other words, a high-energy-barrier event detected at 1000 K can in principle also occur at room temperature, albeit at a much lower frequency. This assumption is based on the observations that all events are spatially localized (See Sec. 6, Supporting Information), and the system undergoes no significant thermally induced changes other than a lattice expansion of 1-3% from the 0 K value.

Next, we post-process our simulation to detect restructuring events. We use a frame rate of $(1\ \mathrm{ps})^{-1}$ for event detection, based on initial visual inspection that most events occur within 1-2 ps, and a 10-times higher frame rate of $(0.1\ \mathrm{ps})^{-1}$ for trajectory extraction after detection. A frame is flagged as an event of potential interest if the z-coordinate of an atom

changes by more than 80% of the average interlayer distance from the value at 1 or 2 ps prior to the said frame. Whenever an exchange event occurs, there is a sharp change in the z-coordinates of the atoms involved, as shown in Fig. 2(a). This criterion is optimized to achieve an event sampling rate of around 100 events within the 20 ns period. If the z-coordinate returns to the original value in the following 1-2 ps, the event is excluded as a thermal attempt. The absolute frequency of the observed events is not expected to be physically accurate due to the empirical nature of the EAM potential, but qualitatively reasonable enough for the purposes of event discovery (See Sec. 7, Supporting Information for the summary of event statistics).

Once the events are detected, we perform visual classification. This choice was mainly due to the relatively small number of the restructuring events observed in our system. Event classification is the only part of our scheme that has not been automated yet. Ongoing work is focusing on fully automating event classification for future application to more complex dynamical systems of interest.[159] Once the events are classified, the corresponding trajectory fragments are further processed through the CI-NEB method, which quenches all thermal fluctuations and allows us to identify suitable initial, transition, and final state candidates for each event. Finally, out of all converged trajectories, we select one representative case from each class and fully optimize it using DFT [Fig. 2(b)]. Event classification guarantees that the events within a given class are highly similar to each other and are essentially described by the same set of microscopic parameters, eliminating the need to optimize all of them.

Results and Discussion

5 main classes of restructuring events

Diffusion at step edges has been extensively investigated due to its central role in determining the island growth mode.[160–163] An adatom at upper edge can either hop over to lower edge, or displace out an edge atom while inserting itself into the edge. The latter case

Table 2: Class 1: Exchange descent. See Fig. 1(a) for illustration of a complete process [case (b)]. Ag/Ag and Pd/Ag refer to the green atom being Ag or Pd, respectively. The transition state and the energy level diagram are fully optimized by DFT. Energy levels are relative to each other only within a given diagram. Energy barriers below 0.60 eV are highlighted in green.

(eV)		Transition state	Ag/Ag	Pd/Ag
A-step	(a)	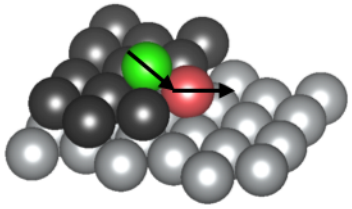	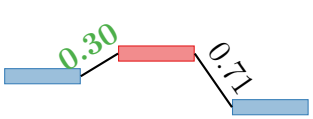	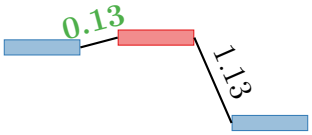
B-step	(b)	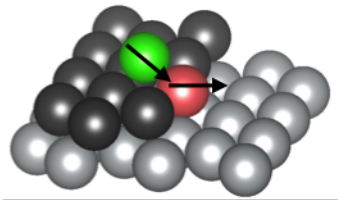	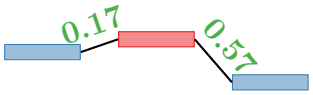	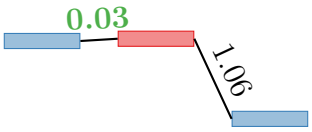
		An adatom (green) descends over the step edge by inserting into the upper edge while pushing out an edge atom (red).		

Upper edge Ag | Lower edge Ag | Pd or Ag in motion | Auxiliary Ag in motion

is the well-established exchange descent (Table 2: Class 1). Whether hopping or exchange dominates ultimately depends on the cohesive energy of the metal. For homoepitaxial case, the net results of hopping and exchange are the same; for heteroepitaxial case, exchange involves heteroatom insertion that is distinct from hopping. In our simulations, we find exchange descent to be the most predominant restructuring event. We only observe exchange rather than hopping, and additional DFT calculations show that exchange has a lower energy barrier than hopping for both Ag/Ag and Pd/Ag (See Sec. 2, Supporting Information for detailed discussion of additional diffusion events at step edges).

There is a coordination loss and activation energy (E_{a}) associated with step descent. The additional activation energy required for the step descent, relative to the terrace diffusion barrier (E_{d}), is known as the Ehrlich-Schwoebel barrier (E_{ES}):[164,165]

$$E_{\mathrm{ES}} = E_{\mathrm{a}} - E_{\mathrm{d}}. \tag{1}$$

We find that exchange descent at B-step is more facile than at A-step, and the corresponding $E_{\mathrm{ES}} = 0.12$ eV for Ag/Ag at B-step is in good agreement with the experimental value of 0.13 eV.[166] This is consistent with our observation that restructuring at B-step is completely dominated by exchange descent (See Sec. 7, Supporting Information), especially at double stairs as observed in previous experiments of rapid vacancy island decay[167,168] (See Sec. 8, Supporting Information for discussion of step doubling phenomenon). As such, we see that the shape of B-step edge is fluid and capable of undergoing extensive restructuring. The exchange descent anisotropy is also in agreement with a previous EAM-KMC study,[160] where non-uniform $E_{\mathrm{ES}}^{\text{B-step}} = \frac{1}{2}E_{\mathrm{ES}}^{\text{A-step}} \approx 0.08$ eV was found to produce simulated morphologies that are consistent with experimental island sizes at 150-180 K.

On the other hand, Pd adatom has a much lower exchange descent barrier than Ag adatom, due to the stronger thermodynamic driving force for Pd to be incorporated into the edge. Notably, the energy barrier is only 0.03 eV for Pd/Ag at B-step, giving $E_{\mathrm{ES}} \approx 0$ eV. We therefore propose exchange descent as the primary way by which Pd adatoms initially become incorporated into the Ag host.

Next, we observe adatom & vacancy generation via popout of surface atoms (Table 3: Class 2). We find that popout always occur via concerted motion, where an auxiliary atom moves along with the atom popping out, leaving behind a vacancy. The auxiliary atom may shift within the same surface layer [cases (a-b)] or push upward from the subsurface layer [cases (c-d)]. Popout can be assisted by a pre-existing adatom [case (b)], where it provides additional coordination and thereby stabilizes the transition state relative to the unassisted case [case (a)]. Assisted popout occurs more frequently than unassisted popout, and the majority of thermal attempts are associated with assisted popout (See Sec. 7, Supporting Information). All popout barriers are higher than 1 eV, with even higher values required for Pd atoms, indicating that popout is a rare event at room temperature.

Insertion, a reverse counterpart of popout, involves an atom moving into the lower edge layer (Table 4: Class 3). The atom being inserted can be either an adatom [cases (a,c,e)]

Table 3: Class 2: Popout. Ag/Ag and Pd/Ag refer to the green atom being Ag or Pd, respectively. The transition state and the energy level diagram are fully optimized by DFT. Energy levels are relative to each other only within a given diagram. Energy barriers below 0.60 eV are highlighted in green.

(eV)	Transition state	Ag/Ag	Pd/Ag
Terrace	(a) 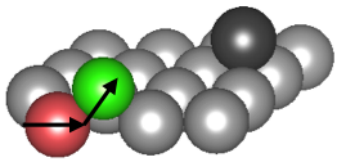	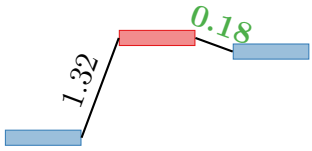	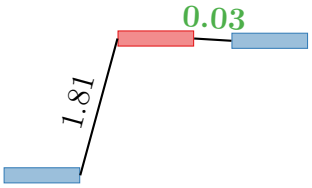
	(b) 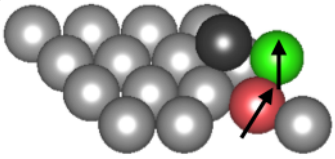	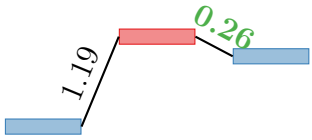	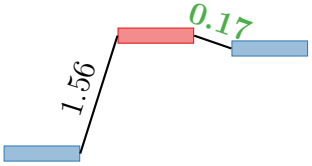
	An atom in the surface layer (green) pops out to the surface, while its original site is claimed by a neighboring auxiliary atom (red). A surface vacancy is created as a result. Case (b) is assisted by a pre-existing adatom (black).		
A-step	(c) 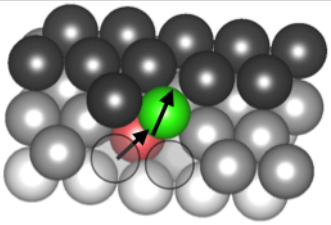	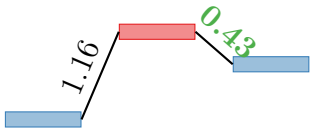	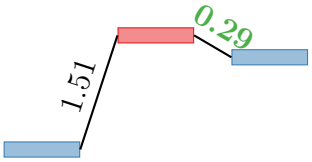
B-step	(d) 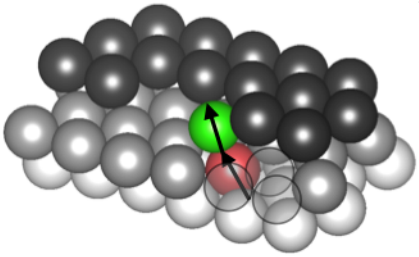	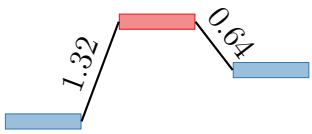	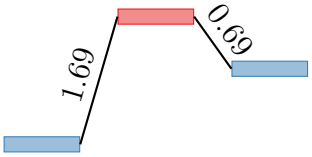
	An atom in the subsurface layer (red) pushes up into the lower edge layer, thereby pushing out an atom in the lower edge layer (green) to the upper edge kink site. A subsurface vacancy is created as a result.		

Upper edge Ag | Lower edge Ag | Subsurface Ag | Pd or Ag in motion | Auxiliary Ag in motion

or part of an edge or a kink site [cases (b,d)]. We consider two types of insertion. Terrace insertion involves a string of auxiliary atoms in the lower terrace that are pushed out toward the next step edge as a result of the insertion [cases (a-b)]. In contrast, vacancy insertion only involves a single auxiliary atom that is pushed into a nearby vacancy [cases (c-e)].

Table 4: Class 3: Terrace & vacancy insertion. Cases (a-b) are terrace insertions; cases (c-e) are vacancy insertions. See Fig. 1(b) for illustration of a complete process for vacancy insertion, case (e). Ag/Ag and Pd/Ag refer to the green atom being Ag or Pd, respectively. The transition state and the energy level diagram are fully optimized by DFT. Energy levels are relative to each other only within a given diagram. Energy barriers below 0.60 eV are highlighted in green.

(eV)		Transition state	Ag/Ag	Pd/Ag
B-step	(a)	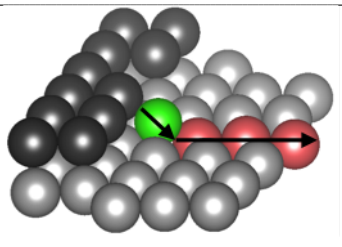	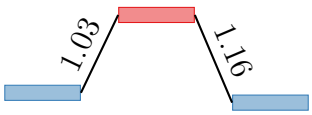	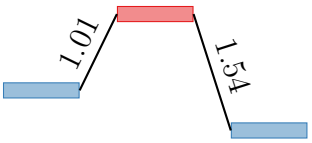
	(b)	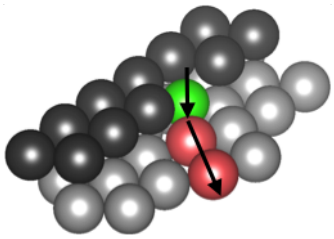	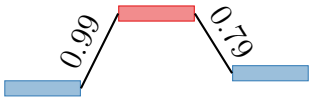	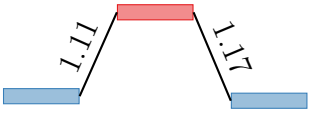
	Terrace insertion: An adatom or an edge atom (green) inserts into the lower edge layer, thereby pushing out a string of auxiliary atoms in the lower terrace (red) toward the next step edge.			
A-step	(c)	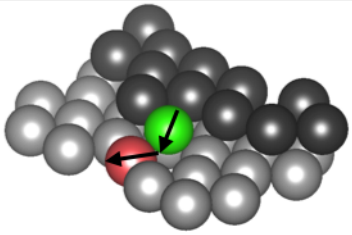	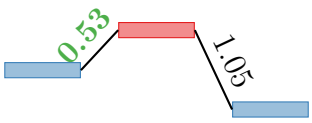	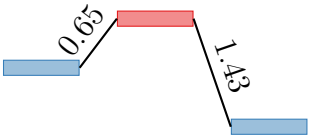
	(d)	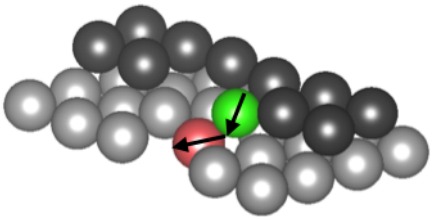	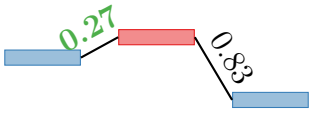	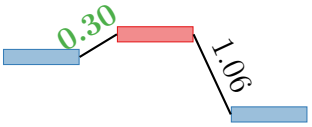
B-step	(e)	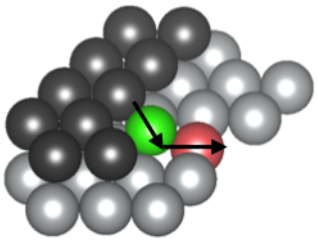	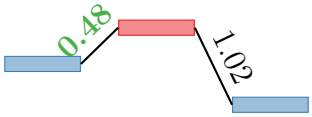	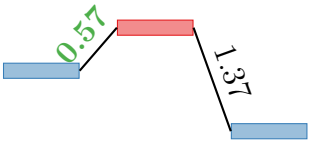
	Vacancy insertion: An adatom or a kink atom (green) inserts into the lower edge layer, while a neighboring auxiliary atom in the lower edge layer (red) is pushed out into a nearby vacancy. Such lower edge vacancies are usually made available in the first place by inward migration of edge vacancies.			

Table 5: Class 4.1: Indirect exchange. Ag/Ag and Pd/Ag refer to the green atom being Ag or Pd, respectively. The transition state and the energy level diagram are fully optimized by DFT. Energy levels are relative to each other only within a given diagram. Energy barriers below 0.60 eV are highlighted in green.

(eV)		Transition state	Ag/Ag	Pd/Ag
Terrace	(a)	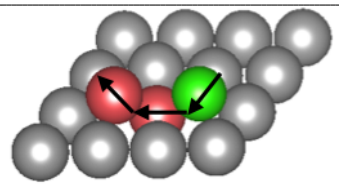	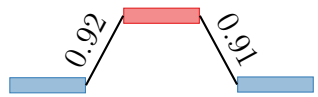	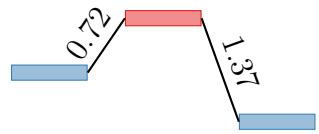
A-step	(b)	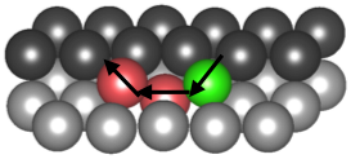	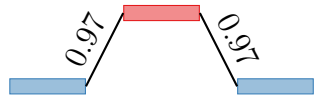	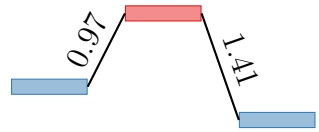
		An adatom (green) inserts into the surface/lower edge layer, thereby pushing out a next-nearest neighboring atom (red) to the surface.		

As expected, vacancy insertion (E_a = 0.3-0.6 eV) is significantly more facile than terrace insertion ($E_a \approx 1.0$ eV). We find that such lower edge vacancies are made available relatively easily in the first place by simple inward migration of edge vacancies (E_a = 0.48 eV).

We next introduce adatom exchange, where an atom in the surface layer is displaced out while another adatom inserts itself into the surface (Table 5-7: Class 4). We distinguish between indirect and direct exchange (Class 4.1 and 4.2, respectively), where an auxiliary atom mediates the exchange in the former. We find that adatom exchange is strained on terraces (E_a = 0.7-1.0 eV), indirect being slightly less strained than direct [cases 4.1(a) & 4.2(a)]. Additional DFT calculations of Pd-Ag direct exchange show similarly high energy barriers on terraces and upper/lower edges, regardless of the number of auxiliary adatoms (See Sec. 3, Supporting Information). The situation remains unchanged at perfect steps, as seen in the case of indirect exchange at A-step [case 4.1(b)].

In contrast, direct exchange barriers are greatly reduced to 0.4-0.6 eV when vacancies and edge atoms are involved at kinks [cases 4.2(b-d)]. At B-step, direct exchange occurs in two stages because the edge close-packing is capable of stabilizing the intermediate lower edge

Table 6: Class 4.2: Direct exchange. See Fig. 1(c) for illustration of a complete process [case (b)]. Two-stage processes are indicated by black arrow first, followed by red arrow, showing the transition state of the second stage. Ag/Ag and Pd/Ag refer to the green atom being Ag or Pd, respectively. The transition state and the energy level diagram are fully optimized by DFT. Energy levels are relative to each other only within a given diagram. Energy barriers below 0.60 eV are highlighted in green.

(eV)		Transition state	Ag/Ag	Pd/Ag
terrace	(a)	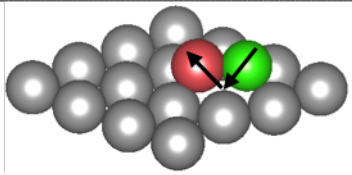	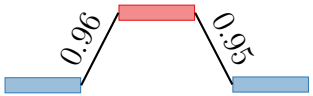	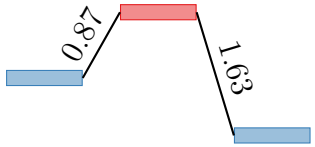
A-step	(b)	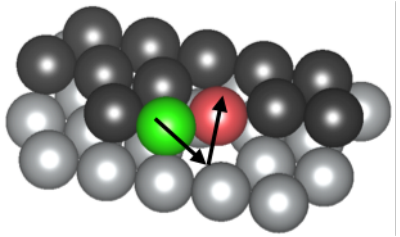	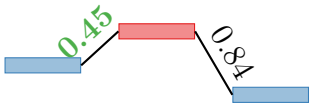	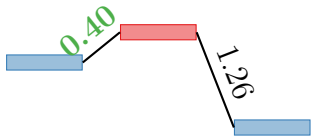
B-step	(c)	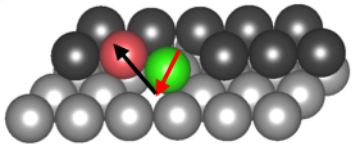	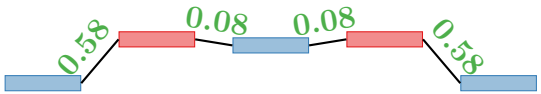	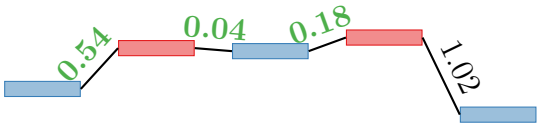
	(d)	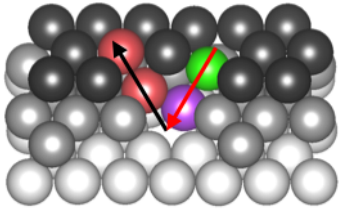	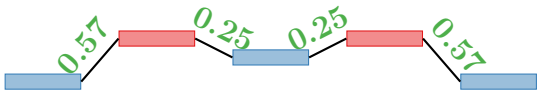	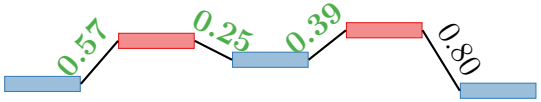

An adatom or an edge atom (green) inserts into the surface/lower edge layer, while a neighboring atom (red) comes up to the surface or into a nearby edge vacancy. The exchange occurs in two stages at B-step [cases (c-d)] because the edge close-packing stabilizes the intermediate lower edge vacancy. Case (d) occurs at double step, involving extra atoms in the middle layer.

Upper edge Ag | Lower edge / middle layer Ag | Lower edge Ag | Pd or Ag in motion | Auxiliary Ag in motion

Table 7: Class 5: Interlayer exchange. See Fig. 1(d) for illustration of a complete process [cases (b-c)]. Ag/Ag and Pd/Ag refer to the green atom being Ag or Pd, respectively. The transition state and the energy level diagram are fully optimized by DFT. Energy levels are relative to each other only within a given diagram. Energy barriers below 0.60 eV are highlighted in green.

(eV)	Transition state	Ag/Ag	Pd/Ag
Terrace	(a) 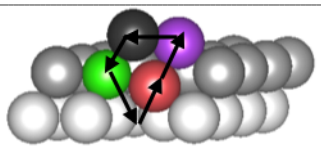	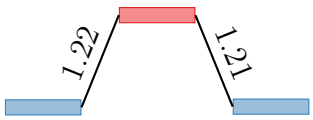	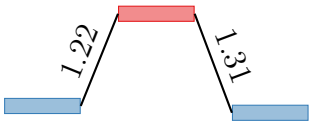
	Concerted rotation involving four atoms: Initially, we have an adatom on the surface (black). An atom in the subsurface layer (red) pushes up into the surface layer, thereby pushing out an atom in the surface layer (purple) to the surface where it joins the pre-existing adatom (black). As a result, a subsurface vacancy is created in the transition state. Afterwards, the neighboring adatom (black) pushes down into the surface layer, thereby pushing down next atom in the surface layer (green) into the subsurface vacancy.		
A-step	(b) 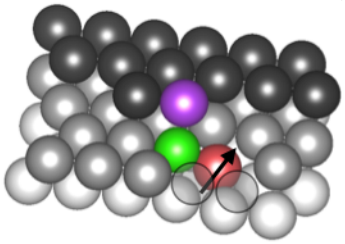		
	(c) 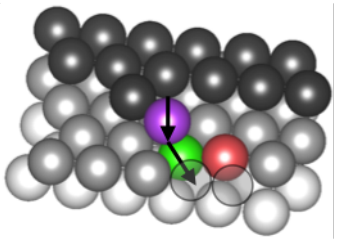	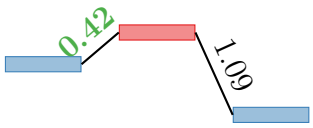	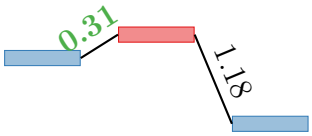
B-step	(d) 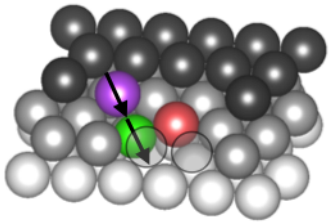	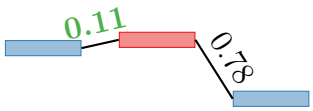	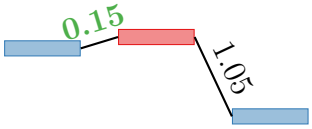
	Initially, we have a vacancy in the lower edge layer. An atom in the subsurface layer (red) pushes up into the lower edge vacancy [case (b)]. A subsurface vacancy is created as a result. Afterwards, a neighboring atom in the lower edge layer (green) inserts into the subsurface vacancy, while its original site is claimed by a nearby adatom (purple) [case (c) for A-step; case (d) for B-step].		

Upper edge Ag | Lower edge Ag | Subsurface Ag | Pd or Ag in motion | Auxiliary Ag in motion

vacancy [cases 4.2(c-d)], which is not the case at A-step [case 4.2(b)]. Interestingly, we find that double steps are also capable of similar process involving multiple atoms [case 4.2(d)]. In the final analysis, we propose direct exchange at kinks as another mechanism by which Pd can be incorporated into the Ag host.

Lastly, we discuss interlayer exchange across surface and subsurface layers (Table 7: Class 5). On terraces, we find that interlayer exchange is a rare event that occurs via concerted rotation of multiple atoms [case (a)]. The process is initiated by a subsurface atom pushing upward into the surface layer, after which a neighboring atom in the surface layer inserts downward into the subsurface. As expected, such concerted rotation is strained ($E_{\mathrm{a}} > 1$ eV). In contrast, interlayer exchange becomes facile at step edges, occurring in two stages with energy barriers below 0.5 eV: A subsurface atom can move up into a lower edge vacancy with ease [case (b)], after which concerted insertion into the subsurface follows [case (c)]. The insertion barrier is particularly low at B-step (< 0.2 eV) [case (d)]. This mechanism is yet another example of how vacancies near steps allow an otherwise strained exchange process to become feasible.

Although the restructuring mechanisms discovered by our event extraction scheme are characterized under vacuum condition, with a focus on Pd incorporation into the Ag host at the single-atom limit, they form an important foundation upon which more complex restructuring phenomena can be investigated, such as Pd/Ag heteroepitaxy.[5] Furthermore, we hypothesize mechanisms similar to the above-mentioned interlayer exchange to be operative for adsorbate-induced Pd reverse segregation. Preliminary DFT calculations show that Pd segregation energy at Ag step edge in the presence of adsorbed H becomes close to zero (-0.02 eV), with a much more negative value (-0.52 eV) in the presence of adsorbed CO, suggesting that surface Pd is capable of being stabilized by these adsorbates (See Sec. 10, Supporting Information). Beyond these thermodynamic insights, ongoing work is focusing on characterizing the restructuring mechanisms in the presence of CO, O, and H to better understand the energetics of reverse segregation. In particular, nontrivial mechanistic co-

operativity may be observed, such as in CO-induced aggregation[123] and surface Pd oxide formation that depends critically on O coverage as well as Pd concentration.[5,121]

Conclusions

Due to the large configurational space intrinsic to surface restructuring phenomena, mechanistic characterization of surface segregation in bimetallic systems using *ab initio* transition state modeling approaches remains scarce and challenging.[89,92,101] In this study, we propose an automated method to map out elementary surface restructuring processes in an unbiased fashion, using Pd/Ag as an example. We utilize high-temperature classical MD simulations to rapidly detect and isolate restructuring events *in vacuo*, which are subsequently optimized using DFT.

In addition to confirming the well-established exchange decent mechanism, our method has revealed three new predominant classes of events at step edges of close-packed surfaces that have not been characterized before: (1) vacancy insertion; (2) direct exchange; (3) interlayer exchange. Our results highlight the importance of vacancies at steps and kinks in facilitating Pd-Ag exchange processes that would otherwise be strained on terraces. Such vacancies are usually made available in the first place by inward migration of edge vacancies. The discovered events enable us to construct the complete set of mechanistic pathways by which Pd is incorporated into the Ag host in vacuum at the single-atom limit. The elementary mechanisms established in our study form an important foundation upon which more complex restructuring phenomena can be investigated, such as Pd/Ag heteroepitaxy[5] as well as possible nontrivial adsorbate effects, such as mechanistic cooperativity in CO-induced aggregation[123] and surface oxide formation.[5,121] Our automated scheme is transferable to other alloy systems of interest and allows the dynamic nature of surfaces to be studied at the microscopic level without losing the first-principles level of accuracy. The atomistic insights presented in our work provide a valuable step toward systematic understanding and engi-

neering of surface segregation in bimetallic catalysts.

Supporting Information Available

Supplementary data is provided for the following: (1) vdW-DFT benchmark of bulk properties; (2) adatom diffusion at step edges of close-packed surface from DFT; (3) direct exchange on close-packed terrace from DFT; (4) EAM potential energetics; (5) adatom diffusion on close-packed terrace from MD; (6) simulation temperature and unit cell size; (7) simulation statistics; (8) step doubling phenomenon; (9) imaginary frequencies of representative transition states; (10) segregation thermodynamics in the presence of adsorbates.

Acknowledgment

This work was supported by the Integrated Mesoscale Architectures for Sustainable Catalysis (IMASC), an Energy Frontier Research Center funded by the US Department of Energy, Office of Science, Office of Basic Energy Sciences under Award No. DE-SC0012573. This research used the following computational resources: (1) the Odyssey cluster, FAS Division of Science, Research Computing Group at Harvard University; (2) the Oak Ridge Leadership Computing Facility, a DOE office of Science User Facility supported under Contract No. DE-AC05-00OR22725, through allocation CHP106; (3) the National Energy Research Scientific Computing Center (NERSC), a DOE Office of Science User Facility supported under Contract No. DE-AC02-05CH11231, through allocation m3275; (4) the Extreme Science and Engineering Discovery Environment (XSEDE),[169] supported by National Science Foundation grant number ACI-1548562, through allocation che170060. We acknowledge enlightening discussions with M. Stamatakis, C. M. Friend, R. J. Madix, E. Kaxiras, W. Chen, L. Sun, and R. Réocreux.

Graphical TOC entry

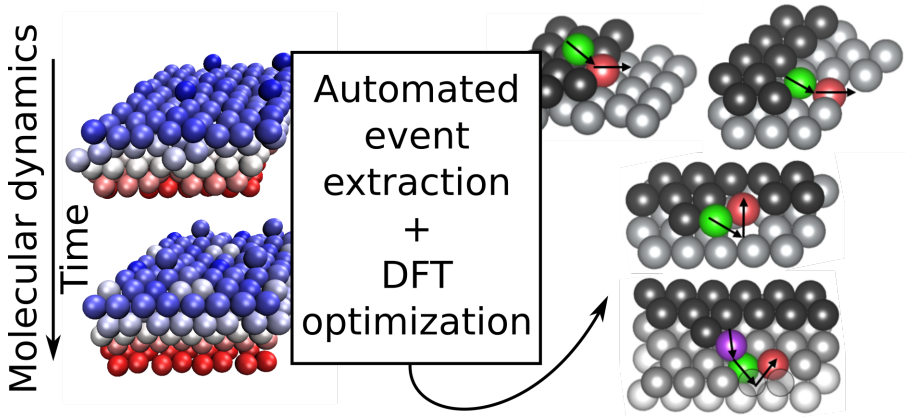

References

(1) Personick, M. L.; Montemore, M. M.; Kaxiras, E.; Madix, R. J.; Biener, J.; Friend, C. M. Catalyst design for enhanced sustainability through fundamental surface chemistry. *Philosophical Transactions of the Royal Society A-Mathematical Physical and Engineering Sciences* **2016**, *374*.

(2) Vignola, E.; Steinmann, S. N.; Al Farra, A.; Vandegehuchte, B. D.; Curulla, D.; Sautet, P. Evaluating the Risk of C-C Bond Formation during Selective Hydrogenation of Acetylene on Palladium. *ACS Catalysis* **2018**, *8*, 1662–1671.

(3) Moskaleva, L.; Chiu, C.-c.; Genest, A.; Roesch, N. Transformations of Organic Molecules over Metal Surfaces: Insights from Computational Catalysis. *Chemical Record* **2016**, *16*, 2388–2404.

(4) Neurock, M. Perspectives on the first principles elucidation and the design of active sites. *Journal of Catalysis* **2003**, *216*, 73–88.

(5) van Spronsen, M. A.; Daunmu, K.; O'Connor, C. R.; Egle, T.; Kersell, H.; Oliver-Meseguer, J.; Salmeron, M. B.; Madix, R. J.; Sautet, P.; Friend, C. M. Dynamics of

Surface Alloys: Rearrangement of Pd/Ag(111) Induced by CO and O-2. *Journal of Physical Chemistry C* **2019**, *123*, 8312–8323.

(6) Vignola, E.; Steinmann, S. N.; Le Mapihan, K.; Vandegehuchte, B. D.; Curulla, D.; Sautet, P. Acetylene Adsorption on Pd-Ag Alloys: Evidence for Limited Island Formation and Strong Reverse Segregation from Monte Carlo Simulations. *Journal of Physical Chemistry C* **2018**, *122*, 15456–15463.

(7) Tao, F. F.; Zhang, S.; Nguyen, L.; Zhang, X. Action of bimetallic nanocatalysts under reaction conditions and during catalysis: evolution of chemistry from high vacuum conditions to reaction conditions. *Chemical Society Reviews* **2012**, *41*, 7980–7993.

(8) Zafeiratos, S.; Piccinin, S.; Teschner, D. Alloys in catalysis: phase separation and surface segregation phenomena in response to the reactive environment. *Catalysis Science & Technology* **2012**, *2*, 1787–1801.

(9) Gilroy, K. D.; Elnabawy, A. O.; Yang, T.-H.; Roling, L. T.; Howe, J.; Mavrikakis, M.; Xia, Y. Thermal Stability of Metal Nanocrystals: An Investigation of the Surface and Bulk Reconstructions of Pd Concave Icosahedra. *Nano Letters* **2017**, *17*, 3655–3661.

(10) Han, Y.; Stoldt, C. R.; Thiel, P. A.; Evans, J. W. Ab Initio Thermodynamics and Kinetics for Coalescence of Two-Dimensional Nanoislands and Nanopits on Metal (100) Surfaces. *Journal of Physical Chemistry C* **2016**, *120*, 21617–21630.

(11) Valcarcel, A.; Loffreda, D.; Delbecq, F.; Piccolo, L. Structure of the Pd8Ni92(110) catalytic surface from first principles. *Physical Review B* **2007**, *76*.

(12) Aspera, S. M.; Arevalo, R. L.; Nakanishi, H.; Kasai, H. First principles study of surface stability and segregation of PdRuRh ternary metal alloy system. *Surface Science* **2018**, *671*, 51–59.

(13) Darby, M. T.; Sykes, E. C. H.; Michaelides, A.; Stamatakis, M. Carbon Monoxide Poisoning Resistance and Structural Stability of Single Atom Alloys. *Topics in Catalysis* **2018**, *61*, 428–438.

(14) Grochola, G.; Snook, I. K.; Russo, S. P. Phase separated reconstruction patterns on strained FCC (111) metal surfaces. *Molecular Simulation* **2016**, *42*, 484–493.

(15) Kim, S. Y.; Lee, I.-H.; Jun, S. Transition-pathway models of atomic diffusion on fcc metal surfaces. II. Stepped surfaces. *Physical Review B* **2007**, *76*.

(16) Zou, L.; Yang, C.; Lei, Y.; Zakharov, D.; Wiezorek, J. M. K.; Su, D.; Yin, Q.; Li, J.; Liu, Z.; Stach, E. A.; et al., Dislocation nucleation facilitated by atomic segregation. *Nature Materials* **2018**, *17*, 56+.

(17) Acharya, S. R.; Rahman, T. S. Toward multiscale modeling of thin-film growth processes using SLKMC. *Journal of Materials Research* **2018**, *33*, 709–719.

(18) Lu, B.; Almyras, G. A.; Gervilla, V.; Greene, J. E.; Sarakinos, K. Formation and morphological evolution of self-similar 3D nanostructures on weakly interacting substrates. *Physical Review Materials* **2018**, *2*.

(19) Cheng, F.; He, X.; Chen, Z.-X.; Huang, Y.-G. Kinetic Monte Carlo simulation of surface segregation in Pd-Cu alloys. *Journal of Alloys and Compounds* **2015**, *648*, 1090–1096.

(20) Kuntova, Z.; Chvoj, Z.; Sima, V.; Tringides, M. C. Limitations of the thermodynamic, Gibbs-Thompson analysis of nanoisland decay. *Physical Review B* **2005**, *71*.

(21) Meunier, I.; Tetot, R.; Treglia, G.; Legrand, B. Thermal dependence of surface polymorphism: the Ag/Cu (111) case. *Applied Surface Science* **2001**, *177*, 252–257, 3rd Porquerolles School on Special Topics in Surface Science, Ile Porquerolles, France, Oct. 01-07, 2000.

(22) Divi, S.; Chatterjee, A. Generalized nano-thermodynamic model for capturing size-dependent surface segregation in multi-metal alloy nanoparticles. *RSC Advances* **2018**, *8*, 10409–10424.

(23) Zhang, P.; Xie, Y.; Ning, X.; Zhuang, J. Equilibrium structures and shapes of clusters on metal fcc(111) surfaces. *Nanotechnology* **2008**, *19*.

(24) Guerrero-Jordan, J.; Luis Cabellos, J.; Johnston, R. L.; Posada-Amarillas, A. Theoretical investigation of the structures of unsupported 38-atom CuPt clusters. *European Physical Journal B* **2018**, *91*.

(25) Shiihara, Y.; Kohyama, M. Contribution of d electrons to surface stresses and their changes by layer relaxation for a series of 4d transition metals. *Surface Science* **2016**, *644*, 122–128.

(26) Rost, M. J.; van Albada, S. B.; Frenken, J. W. M. Shape and evolution of vacancy islands on a missing row reconstructed surface: Au(110). *Surface Science* **2002**, *518*, 21–38.

(27) Bach, C. E.; Giesen, M.; Ibach, H.; Einstein, T. L. Stress relief in reconstruction. *Physical Review Letters* **1997**, *78*, 4225–4228.

(28) Koch, R.; Borbonus, M.; Haase, O.; Rieder, K. H. Reconstruction behavior of FCC(110) transition-metal surfaces and their vicinals. *Applied Physics A-Materials Science & Processing* **1992**, *55*, 417–429.

(29) Thiel, P. A.; Shen, M.; Liu, D.-J.; Evans, J. W. Coarsening of Two-Dimensional Nanoclusters on Metal Surfaces. *Journal of Physical Chemistry C* **2009**, *113*, 5047–5067.

(30) Roussel, J. M.; Saul, A.; Treglia, G.; Legrand, B. Layer-by-layer versus surfactant dissolution modes in heteroepitaxy. *Physical B* **1999**, *60*, 13890–13901.

(31) Treglia, G.; Legrand, B.; Ducastelle, F.; Saul, A.; Gallis, C.; Meunier, I.; Mottet, C.; Senhaji, A. Alloy surfaces: segregation, reconstruction and phase transitions. *Computational Materials Science* **1999**, *15*, 196–235.

(32) Giannakakis, G.; Flytzani-Stephanopoulos, M.; Sykes, E. C. H. Single-Atom Alloys as a Reductionist Approach to the Rational Design of Heterogeneous Catalysts. *Accounts of Chemical Research* **2019**, *52*, 237–247.

(33) Vile, G.; Albani, D.; Almora-Barrios, N.; Lopez, N.; Perez-Ramirez, J. Advances in the Design of Nanostructured Catalysts for Selective Hydrogenation. *ChemCatChem* **2016**, *8*, 21–33.

(34) McCue, A. J.; Anderson, J. A. Recent advances in selective acetylene hydrogenation using palladium containing catalysts. *Frontiers of Chemical Science and Engineering* **2015**, *9*, 142–153.

(35) Liao, F.; Lo, T. W. B.; Tsang, S. C. E. Recent Developments in Palladium-Based Bimetallic Catalysts. *ChemCatChem* **2015**, *7*, 1998–2014.

(36) Nikolaev, S. A.; Zanaveskin, L. N.; Smirnov, V. V.; Averyanov, V. A.; Zanaveskin, K. L. Catalytic hydrogenation of alkyne and alkadiene impurities in alkenes. Practical and theoretical aspects. *Russian Chemical Reviews* **2009**, *78*, 231–247.

(37) Coq, B.; Figueras, F. Bimetallic palladium catalysts: influence of the co-metal on the catalyst performance. *Journal of Molecular Catalysis A-Chemical* **2001**, *173*, 117–134.

(38) Jeong, G.-U.; Park, C. S.; Do, H.-S.; Park, S.-M.; Lee, B.-J. Second nearest-neighbor modified embedded-atom method interatomic potentials for the Pd-M (M = Al, Co, Cu, Fe, Mo, Ni, Ti) binary systems. *Calphad-Computer Coupling of Phase Diagrams and Thermochemistry* **2018**, *62*, 172–186.

(39) Mottet, C.; Treglia, G.; Legrand, B. Theoretical investigation of chemical and morphological ordering in PdcCu1-c clusters. *Physical Review B* **2002**, *66*.

(40) Yang, L. Q. Reverse surface segregation in Cu-Pd bimetallic catalysts at low concentrations of Cu. *Philosophical Magazine A-Physics of Condensed Matter Structure Defects and Mechanical Properties* **2000**, *80*, 1879–1888.

(41) Shah, V.; Yang, L. Q. Nanometre fcc clusters versus bulk bcc alloy: the structure of Cu-Pd catalysts. *Philosophical Magazine A-Physics of Condensed Matter Structure Defects and Mechanical Properties* **1999**, *79*, 2025–2049.

(42) Deurinck, P.; Creemers, C. Monte Carlo simulation of Cu segregation and ordering at the (110) surface of Cu75Pd25. *Surface Science* **1998**, *419*, 62–77.

(43) Christensen, A.; Ruban, A. V.; Stoltze, P.; Jacobsen, K. W.; Skriver, H. L.; Norskov, J. K.; Besenbacher, F. Phase diagrams for surface alloys. *Physical Review B* **1997**, *56*, 5822–5834.

(44) Yang, L. Q.; DePristo, A. E. Surface segregation in bimetallic clusters - statistical-mechanical modeling using cluster site energies. *Journal of Catalysis* **1994**, *148*, 575–586.

(45) Logsdail, A. J.; Oliver Paz-Borbon, L.; Downing, C. A. DFT-Computed Trends in the Properties of Bimetallic Precious Metal Nanoparticles with Core@Shell Segregation. *Journal of Physical Chemistry C* **2018**, *122*, 5721–5730.

(46) Yaghoubi, H. Melting Properties and Structural Evolution of (AgxPd1-x)(256) Bimetallic Nanoclusters Supported on SWCNT: A Molecular Dynamics Simulation. *Journal of Molecular Liquids* **2017**, *230*, 305–314.

(47) Hewage, J. W. Core/shell formation and surface segregation of multi shell icosahedral

silver-palladium bimetallic nanostructures: A dynamic and thermodynamic study. *Materials Chemistry and Physics* **2016**, *174*, 187–194.

(48) Bochicchio, D.; Ferrando, R.; Novakovic, R.; Panizon, E.; Rossi, G. Chemical ordering in magic-size Ag-Pd nanoparticles. *Physical Chemistry Chemical Physics* **2014**, *16*, 26478–26484.

(49) Tang, J.; Deng, L.; Deng, H.; Xiao, S.; Zhang, X.; Hu, W. Surface Segregation and Chemical Ordering Patterns of Ag-Pd Nanoalloys: Energetic Factors, Nanoscale Effects, and Catalytic Implication. *Journal of Physical Chemistry C* **2014**, *118*, 27850–27860.

(50) Aguilera-Granja, F.; Piotrowski, M. J.; da Silva, J. L. F. Structural and electronic properties of TM23-pAgp (TM = Ni, Pd, and Pt) clusters in the dilute limit (p=0-4): A density functional theory investigation. *European Physical Journal D* **2013**, *67*.

(51) Xiao, X.; Shi, D.; Xia, J.; Cheng, Z. Influence of initial temperatures on the cooling of Ag-Pd bimetallic clusters via molecular dynamics simulation. *Nano* **2013**, *8*.

(52) Li, G.; Wang, Q.; Liu, T.; Wang, K.; Wu, C.; He, J. Controllable irregular phenomenon induced by Ag atomic segregation on the melting of (AgPd)(561) bimetallic clusters. *Journal of Nanoparticle Research* **2012**, *14*.

(53) Kim, H. Y.; Kim, D. H.; Lee, H. M. Temperature and Composition Dependent Structural Evolution of AgPd Bimetallic Nanoparticle: Phase Diagram of (AgPd)(151) Nanoparticle. *Journal of Nanoscience and Nanotechnology* **2011**, *11*, 2251–2255.

(54) Wu, X.; Wu, Y.; Kai, X.; Wu, G.; Chen, Y. Structural optimization of Ag-Pd clusters based on different potential parameterizations. *Chemical Physics* **2011**, *390*, 36–41.

(55) Chen, C.-K.; Chang, S.-C.; Chen, C.-L. Molecular dynamics simulations of the inter-

nal temperature dependent diffusing and epitaxial behaviors of Pd-Ag cluster beam deposition. *Journal of Applied Physics* **2010**, *107*.

(56) Xiao, X.-Y. Irregular phenomenon induced by Ag atomic segregation during the heating process of Ag-Pd cluster. *Chinese Physics B* **2010**, *19*.

(57) Kim, H. Y.; Kim, H. G.; Kim, D. H.; Lee, H. M. Overstabilization of the Metastable Structure of Isolated Ag-Pd Bimetallic Clusters. *Journal of Physical Chemistry C* **2008**, *112*, 17138–17142.

(58) Marten, T.; Hellman, O.; Ruban, A. V.; Olovsson, W.; Kramer, C.; Godowski, J. P.; Bech, L.; Li, Z.; Onsgaard, J.; Abrikosov, I. A. Double-segregation effect in AgxPd1-x/Ru(0001) thin film nanostructures. *Physical Review B* **2008**, *77*.

(59) Kim, H. Y.; Kim, H. G.; Ryu, J. H.; Lee, H. M. Preferential segregation of Pd atoms in the Ag-Pd bimetallic cluster: Density functional theory and molecular dynamics simulation. *Physical Review B* **2007**, *75*.

(60) Kim, H. Y.; Lee, S. H.; Kim, H. G.; Ryu, J. H.; Lee, H. M. Molecular dynamic simulation of coalescence between silver and palladium clusters. *Materials Transactions* **2007**, *48*, 455–459.

(61) Ruban, A. V.; Simak, S. I.; Korzhavyi, P. A.; Johansson, B. Theoretical investigation of bulk ordering and surface segregation in Ag-Pd and other isoelectornic alloys. *Physical Review B* **2007**, *75*.

(62) Zhang, J.-M.; Wang, B.; Xu, K.-W. Surface segregation of the metal impurity to the (100) surface of fcc metals. *Pramana-Journal of Physics* **2007**, *69*, 603–616.

(63) Ropo, M. Ab initio study of the geometric dependence of AgPd surface segregation. *Physical Review B* **2006**, *74*.

(64) Ropo, M.; Kokko, K.; Vitos, L.; Kollar, J.; Johansson, B. The chemical potential in surface segregation calculations: AgPd alloys. *Surface Science* **2006**, *600*, 904–913.

(65) Baletto, F.; Mottet, C.; Ferrando, R. Time evolution of Ag-Cu and Ag-Pd core-shell nanoclusters. *European Physical Journal D* **2003**, *24*, 233–236, 11th International Symposium on Small Particles and Inorganic Clusters (ISSPIC 11), Strasbourg, France, Sep. 09-13, 2002.

(66) Baletto, F.; Mottet, C.; Ferrando, R. Growth simulations of silver shells on copper and palladium nanoclusters. *Physical Review B* **2002**, *66*.

(67) Drchal, V.; Pasturel, A.; Monnier, R.; Kudrnovsky, J.; Weinberger, P. Theory of surface segregation in metallic alloys: The generalized perturbation method. *Computational Materials Science* **1999**, *15*, 144–168.

(68) Bozzolo, G.; Good, B.; Ferrante, J. Heat of segregation of single substitutional impurities. *Surface Science* **1993**, *289*, 169–179.

(69) Gijzeman, O. L. J. Surface segregation in small supported particles. *Applied Surface Science* **1993**, *64*, 9–20.

(70) Deng, L.; Zhang, X.; Wang, L.; Tang, J.; Liu, Z.; Xiao, S.; Deng, H.; Hu, W. Local identification of chemical ordering: Extension, implementation, and application of the common neighbor analysis for binary systems. *Computational Materials Science* **2018**, *143*, 195–205.

(71) Akbarzadeh, H.; Mehrjouei, E.; Sherafati, M.; Shamkhali, A. N. Dumbbell-like, core-shell and Janus-like configurations in Pd@Au@Pd three-shell nanoalloys: a molecular dynamics study. *Inorganic Chemistry Frontiers* **2017**, *4*, 1551–1561.

(72) Boes, J. R.; Kitchin, J. R. Modeling Segregation on AuPd(111) Surfaces with Density

Functional Theory and Monte Carlo Simulations. *Journal of Physical Chemistry C* **2017**, *121*, 3479–3487.

(73) Zhu, B.; Front, A.; Guesmi, H.; Creuze, J.; Legrand, B.; Mottet, C. Magic compositions in Pd-Au nanoalloys. *Computational and Theoretical Chemistry* **2017**, *1107*, 49–56.

(74) Creuze, J.; Guesmi, H.; Mottet, C.; Zhu, B.; Legrand, B. Surface segregation in AuPd alloys: Ab initio analysis of the driving forces. *Surface Science* **2015**, *639*, 48–53.

(75) Gui-Fang, S.; Wen-Xin, Z.; Na-Na, T.; Tun-Dong, L.; Yu-Hua, W. Investigation on stable structures of Au-Pd alloy nanoparticles with high-index facets. *Acta Physica Sinica* **2015**, *64*.

(76) Zhu, B.; Guesmi, H.; Creuze, J.; Legrand, B.; Mottet, C. Crossover among structural motifs in Pd-Au nanoalloys. *Physical Chemistry Chemical Physics* **2015**, *17*, 28129–28136.

(77) Ismail, R.; Ferrando, R.; Johnston, R. L. Theoretical Study of the Structures and Chemical Ordering of Palladium-Gold Nanoalloys Supported on MgO(100). *Journal of Physical Chemistry C* **2013**, *117*, 293–301.

(78) Zhu, B.; Wang, Y.; Atanasov, I. S.; Cheng, D.; Hou, M. Ordering and segregation in isolated Au-Pd icosahedral nanoclusters and nanowires and the consequences of their encapsulation inside carbon nanotubes. *Journal of Physics D-Applied Physics* **2012**, *45*.

(79) Fratesi, G. First-principles investigation of the early stages of Pd adsorption on Au(111). *Journal of Physics-Condensed Matter* **2011**, *23*.

(80) Atanasov, I.; Hou, M. Thermodynamic properties of Au-Pd nanostructured surfaces studied by atomic scale modelling. Physica Status Solidi C: Current Topics in Solid

State Physics, Vol. 7, No. 11-12. 2010; pp 2604–2607, 10th International Conference on Trends in Nanotechnology (TNT), Barcelona, Spain, Sep. 07-11, 2009.

(81) Ismail, R.; Johnston, R. L. Investigation of the structures and chemical ordering of small Pd-Au clusters as a function of composition and potential parameterisation. *Physical Chemistry Chemical Physics* **2010**, *12*, 8607–8619.

(82) Atanasov, I.; Hou, M. Equilibrium ordering properties of Au-Pd alloys and nanoalloys. *Surface Science* **2009**, *603*, 2639–2651.

(83) Pittaway, F.; Paz-Borbon, L. O.; Johnston, R. L.; Arslan, H.; Ferrando, R.; Mottet, C.; Barcaro, G.; Fortunelli, A. Theoretical Studies of Palladium-Gold Nanoclusters: Pd-Au Clusters with up to 50 Atoms. *Journal of Physical Chemistry C* **2009**, *113*, 9141–9152.

(84) Yuan, D.; Gong, X.; Wu, R. Peculiar distribution of Pd on Au nanoclusters: First-principles studies. *Physical Review B* **2008**, *78*.

(85) Chen, Y.; Liao, S. Monte Carlo simulation of the surface segregation of Au75Pd25 at (110) surface using an analytic embedded atom method. *Surface Review and Letters* **2007**, *14*, 411–417.

(86) Creemers, C.; Deurinck, P. Platinum segregation to the (111) surface of ordered Pt80Fe20: LEIS results and model simulations. *Surface and Interface Analysis* **1997**, *25*, 177–190, QSA-9 Conference, Guildford, England, Jul. 15-19, 1996.

(87) Creemers, C.; Hove, H. V.; Neyens, A. Low-energy ion-scattering study of Be and Sn segregation in their alloys with Cu. *Applied Surface Science* **1981**, *7*, 402–418.

(88) Hirschl, R.; Delbecq, F.; Sautet, P.; Hafner, J. Adsorption of unsaturated aldehydes on the (111) surface of a Pt-Fe alloy catalyst from first principles. *Journal of Catalysis* **2003**, *217*, 354–366.

(89) Yang, Yongpeng and Shen, Xiangjian and Han, Yi-Fan, Diffusion mechanisms of metal atoms in PdAu bimetallic catalyst under CO atmosphere based on ab initio molecular dynamics. *Applied Surface Science* **2019**, *483*, 991–1005.

(90) Goulas, K. A.; Song, Y.; Johnson, G. R.; Chen, J. P.; Gokhale, A. A.; Grabow, L. C.; Toste, F. D. Selectivity tuning over monometallic and bimetallic dehydrogenation catalysts: effects of support and particle size. *Catalysis Science & Technology* **2018**, *8*, 314–327.

(91) Oguz, I. C.; Mineva, T.; Creuze, J.; Guesmi, H. Equilibrium Au-Pd(100) Surface Structures under CO Pressure: Energetic Stabilities and Phase Diagrams. *Journal of Physical Chemistry C* **2018**, *122*, 18922–18932.

(92) An, H.; Ha, H.; Yoo, M.; Kim, H. Y. Understanding the atomic-level process of CO-adsorption-driven surface segregation of Pd in (AuPd)(147) bimetallic nanoparticles. *Nanoscale* **2017**, *9*, 12077–12086.

(93) Padama, A. A. B.; Villaos, R. A. B.; Albia, J. R.; Dino, W. A.; Nakanishi, H.; Kasai, H. CO-induced Pd segregation and the effect of subsurface Pd on CO adsorption on CuPd surfaces. *Journal of Physics-Condensed Matter* **2017**, *29*.

(94) Padama, A. A. B.; Cristobal, A. P. S.; Ocon, J. D.; Dino, W. A.; Kasai, H. Effects of Adsorbates (CO, COH, and HCO) on the Arrangement of Pd Atoms in PdCu(111). *Journal of Physical Chemistry C* **2017**, *121*, 17818–17826.

(95) Fernandes, V. R.; Van den Bossche, M.; Knudsen, J.; Farstad, M. H.; Gustafson, J.; Venvik, H. J.; Gronbeck, H.; Borg, A. Reversed Hysteresis during CO Oxidation over Pd75Ag25(100). *ACS Catalysis* **2016**, *6*, 4154–4161.

(96) Zhu, B.; Creuze, J.; Mottet, C.; Legrand, B.; Guesmi, H. CO Adsorption-Induced Surface Segregation and Formation of Pd Chains on AuPd(100) Alloy: Density Func-

tional Theory Based Ising Model and Monte Carlo Simulations. *Journal of Physical Chemistry C* **2016**, *120*, 350–359.

(97) Anicijevic, D. D. V.; Nikolic, V. M.; Kaninski, M. P. M.; Pasti, I. A. Structure, chemisorption properties and electrocatalysis by Pd3Au overlayers on tungsten carbide - A DFT study. *International Journal of Hydrogen Energy* **2015**, *40*, 6085–6096.

(98) Saqlain, M. A.; Hussain, A.; Siddiq, M.; Leitao, A. A. Synergy between Pd and Au in a Pd-Au(100) bimetallic surface for the water gas shift reaction: a DFT study. *RSC Advances* **2015**, *5*, 47066–47073.

(99) Li, M.; Li, S.; Cheng, D. Influence of adsorbates on the segregation properties of Au-Pd bimetallic clusters. *Computational Materials Science* **2014**, *81*, 253–258.

(100) Sansa, M.; Dhouib, A.; Guesmi, H. Density functional theory study of CO-induced segregation in gold-based alloys. *Journal of Chemical Physics* **2014**, *141*.

(101) Kim, H. Y.; Henkelman, G. CO Adsorption-Driven Surface Segregation of Pd on Au/Pd Bimetallic Surfaces: Role of Defects and Effect on CO Oxidation. *ACS Catalysis* **2013**, *3*, 2541–2546.

(102) West, P. S.; Johnston, R. L.; Barcaro, G.; Fortunelli, A. Effect of CO and H adsorption on the compositional structure of binary nanoalloys via DFT modeling. *European Physical Journal D* **2013**, *67*.

(103) Zhu, B.; Thrimurthulu, G.; Delannoy, L.; Louis, C.; Mottet, C.; Creuze, J.; Legrand, B.; Guesmi, H. Evidence of Pd segregation and stabilization at edges of AuPd nano-clusters in the presence of CO: A combined DFT and DRIFTS study. *Journal of Catalysis* **2013**, *308*, 272–281.

(104) Ham, H. C.; Stephens, J. A.; Hwang, G. S.; Han, J.; Nam, S. W.; Lim, T. H. Role of

Small Pd Ensembles in Boosting CO Oxidation in AuPd Alloys. *Journal of Physical Chemistry Letters* **2012**, *3*, 566–570.

(105) Svenum, I.-H.; Herron, J. A.; Mavrikakis, M.; Venvik, H. J. Adsorbate-induced segregation in a PdAg membrane model system: Pd3Ag(111). *Catalysis Today* **2012**, *193*, 111–119, 10th International Conference on Catalysis in Membrane Reactors, Saint-Petersburg, Russia, Jun. 20-24, 2011.

(106) Abbott, H. L.; Aumer, A.; Lei, Y.; Asokan, C.; Meyer, R. J.; Sterrer, M.; Shaikhutdinov, S.; Freund, H.-J. CO Adsorption on Monometallic and Bimetallic Au-Pd Nanoparticles Supported on Oxide Thin Films. *Journal of Physical Chemistry C* **2010**, *114*, 17099–17104.

(107) Garcia-Mota, M.; Lopez, N. Temperature and pressure effects in CO titration of ensembles in PdAu(111) alloys using first principles. *Physical Review B* **2010**, *82*.

(108) West, P. S.; Johnston, R. L.; Barcaro, G.; Fortunelli, A. The Effect of CO and H Chemisorption on the Chemical Ordering of Bimetallic Clusters. *Journal of Physical Chemistry C* **2010**, *114*, 19678–19686.

(109) Soto-Verdugo, V.; Metiu, H. Segregation at the surface of an Au/Pd alloy exposed to CO. *Surface Science* **2007**, *601*, 5332–5339.

(110) Czelej, K.; Cwieka, K.; Colmenares, J. C.; Kurzydlowski, K. J.; Xu, Y.-J. Toward a Comprehensive Understanding of Enhanced Photocatalytic Activity of the Bimetallic PdAu/TiO2 Catalyst for Selective Oxidation of Methanol to Methyl Formate. *ACS Applied Materials & Interfaces* **2017**, *9*, 31825–31833.

(111) Tripkovic, V.; Hansen, H. A.; Rossmeisl, J.; Vegge, T. First principles investigation of the activity of thin film Pt, Pd and Au surface alloys for oxygen reduction. *Physical Chemistry Chemical Physics* **2015**, *17*, 11647–11657.

(112) Dhouib, A.; Guesmi, H. DFT study of the M segregation on MAu alloys (M = Ni, Pd, Pt) in presence of adsorbed oxygen O and O-2. *Chemical Physics Letters* **2012**, *521*, 98–103.

(113) Jirkovsky, J. S.; Panas, I.; Romani, S.; Ahlberg, E.; Schiffrin, D. J. Potential-Dependent Structural Memory Effects in Au-Pd Nanoalloys. *Journal of Physical Chemistry Letters* **2012**, *3*, 315–321.

(114) Walle, L. E.; Gronbeck, H.; Fernandes, V. R.; Blomberg, S.; Farstad, M. H.; Schulte, K.; Gustafson, J.; Andersen, J. N.; Lundgren, E.; Borg, A. Surface composition of clean and oxidized Pd75Ag25(100) from photoelectron spectroscopy and density functional theory calculations. *Surface Science* **2012**, *606*, 1777–1782.

(115) Guesmi, H.; Louis, C.; Delannoy, L. Chemisorbed atomic oxygen inducing Pd segregation in PdAu(111) alloy: Energetic and electronic DFT analysis. *Chemical Physics Letters* **2011**, *503*, 97–100.

(116) Kitchin, J. R.; Reuter, K.; Scheffler, M. Alloy surface segregation in reactive environments: First-principles atomistic thermodynamics study of Ag3Pd(111) in oxygen atmospheres. *Physical Review B* **2008**, *77*.

(117) Xu, C.-Q.; Lee, M.-S.; Wang, Y.-G.; Cantu, D. C.; Li, J.; Glezakou, V.-A.; Rousseau, R. Structural Rearrangement of Au-Pd Nanoparticles under Reaction Conditions: An ab Initio Molecular Dynamics Study. *ACS Nano* **2017**, *11*, 1649–1658.

(118) Boes, J. R.; Gumuslu, G.; Miller, J. B.; Gellman, A. J.; Kitchin, J. R. Estimating Bulk-Composition-Dependent H-2 Adsorption Energies on CuxPd1-x, Alloy (111) Surfaces. *ACS Catalysis* **2015**, *5*, 1020–1026.

(119) Lovvik, O. M.; Opalka, S. M. Reversed surface segregation in palladium-silver alloys due to hydrogen adsorption. *Surface Science* **2008**, *602*, 2840–2844.

(120) Gonzalez, S.; Neyman, K. M.; Shaikhutdinov, S.; Freund, H.-J.; Illas, F. On the promoting role of Ag in selective hydrogenation reactions over Pd-Ag bimetallic catalysts: A theoretical study. *Journal of Physical Chemistry C* **2007**, *111*, 6852–6856.

(121) Wexler, R. B.; Qiu, T.; Rappe, A. M. Automatic Prediction of Surface Phase Diagrams Using Ab lnitio Grand Canonical Monte Carlo. *Journal of Physical Chemistry C* **2019**, *123*, 2321–2328.

(122) Vignola, E.; Steinmann, S. N.; Vandegehuchte, B. D.; Curulla, D.; Sautet, P. C2H2-Induced Surface Restructuring of Pd-Ag Catalysts: Insights from Theoretical Modeling. *Journal of Physical Chemistry C* **2016**, *120*, 26320–26327.

(123) Michalka, J. R.; Gezelter, J. D. Island Formation on Pt/Pd(557) Surface Alloys in the Presence of Adsorbed CO: A Molecular Dynamics Study. *Journal of Physical Chemistry C* **2015**, *119*, 14239–14247.

(124) Hohenberg, P.; Kohn, W. Inhomogeneous electron gas. *Physical Review B* **1964**, *136*, B864+.

(125) Kresse, G.; Furthmuller, J. Efficient iterative schemes for ab initio total-energy calculations using a plane-wave basis set. *Physical Review B* **1996**, *54*, 11169–11186.

(126) Blochl, P. E. Projector augmented-wave method. *Physical Review B* **1994**, *50*, 17953–17979.

(127) Kresse, G.; Joubert, D. From ultrasoft pseudopotentials to the projector augmented-wave method. *Physical Review B* **1999**, *59*, 1758–1775.

(128) Kresse, G. Ab-initio molecular-dynamics for liquid-metals. *Journal of Non-Crystalline Solids* **1995**, *193*, 222–229.

(129) Methfessel, M.; Paxton, A. T. High-precision sampling for Brillouin-zone integration in metals. *Physical Review B* **1989**, *40*, 3616–3621.

(130) Henkelman, G.; Jonsson, H. A dimer method for finding saddle points on high dimensional potential surfaces using only first derivatives. *Journal of Chemical Physics* **1999**, *111*, 7010–7022.

(131) http://theory.cm.utexas.edu/vtsttools/.

(132) Murnaghan, F. D. The compressibility of media under extreme pressures. *Proceedings of the National Academy of Sciences of the United States of America* **1944**, *30*, 244–247.

(133) BIRCH, F. Finite elastic strain of cubic crystals. *Physical Review* **1947**, *71*, 809–824.

(134) Grimme, S.; Antony, J.; Ehrlich, S.; Krieg, H. A consistent and accurate ab initio parametrization of density functional dispersion correction (DFT-D) for the 94 elements H-Pu. *Journal of Chemical Physics* **2010**, *132*.

(135) Tkatchenko, A.; Scheffler, M. Accurate Molecular Van Der Waals Interactions from Ground-State Electron Density and Free-Atom Reference Data. *Physical Review Letters* **2009**, *102*.

(136) Steinmann, S. N.; Corminboeuf, C. A generalized-gradient approximation exchange hole model for dispersion coefficients. *Journal of Chemical Physics* **2011**, *134*.

(137) Steinmann, S. N.; Corminboeuf, C. Comprehensive Bench marking of a Density-Dependent Dispersion Correction. *Journal of Chemical Theory and Computation* **2011**, *7*, 3567–3577.

(138) Dion, M.; Rydberg, H.; Schroder, E.; Langreth, D. C.; Lundqvist, B. I. Van der Waals density functional for general geometries. *Physical Review Letters* **2004**, *92*.

(139) Roman-Perez, G.; Soler, J. M. Efficient Implementation of a van der Waals Density Functional: Application to Double-Wall Carbon Nanotubes. *Physical Review Letters* **2009**, *103*.

(140) Klimes, J.; Bowler, D. R.; Michaelides, A. Chemical accuracy for the van der Waals density functional. *Journal of Physics-Condensed Matter* **2010**, *22*.

(141) Lee, K.; Murray, E. D.; Kong, L.; Lundqvist, B. I.; Langreth, D. C. Higher-accuracy van der Waals density functional. *Physical Review B* **2010**, *82*.

(142) Klimes, J.; Bowler, D. R.; Michaelides, A. Van der Waals density functionals applied to solids. *Physical Review B* **2011**, *83*.

(143) Perdew, J. P.; Burke, K.; Ernzerhof, M. Generalized gradient approximation made simple. *Physical Review Letters* **1996**, *77*, 3865–3868.

(144) Feng, D.; Taskinen, P. Thermodynamic properties of silver-palladium alloys determined by a solid state electrochemical method. *Journal of Materials Science* **2014**, *49*, 5790–5798.

(145) Plimpton, S. Fast Parallel Algorithms for short-range molecular-dynamics. *Journal of Computational Physics* **1995**, *117*, 1–19.

(146) Hale, L. M.; Wong, B. M.; Zimmerman, J. A.; Zhou, X. W. Atomistic potentials for palladium-silver hydrides. *Modelling and Simulation in Materials Science and Engineering* **2013**, *21*.

(147) Hoover, W. G. Canonical dynamics - equilibrium phase-space distributions. *Physical Review A* **1985**, *31*, 1695–1697.

(148) Nose, S. A unified formulation of the constant temperature molecular-dynamics methods. *Journal of Chemical Physics* **1984**, *81*, 511–519.

(149) Hoover, W. G. Constant-pressure equations of motion. *Physical Review A* **1986**, *34*, 2499–2500.

(150) Henkelman, G.; Jonsson, H. Improved tangent estimate in the nudged elastic band method for finding minimum energy paths and saddle points. *Journal of Chemical Physics* **2000**, *113*, 9978–9985.

(151) Henkelman, G.; Uberuaga, B. P.; Jonsson, H. A climbing image nudged elastic band method for finding saddle points and minimum energy paths. *Journal of Chemical Physics* **2000**, *113*, 9901–9904.

(152) Thirumalai, H.; Kitchin, J. R. Investigating the Reactivity of Single Atom Alloys Using Density Functional Theory. *Topics in Catalysis* **2018**, *61*, 462–474.

(153) Williams, P. L.; Mishin, Y.; Hamilton, J. C. An embedded-atom potential for the Cu-Ag system. *Modelling and Simulation in Materials Science and Engineering* **2006**, *14*, 817–833.

(154) Kittel, C. *Introduction to Solid State Physics*, 8th ed.; Wiley, 2004.

(155) Liang, T.; Zhou, D.; Wu, Z.; Shi, P. Size-dependent melting modes and behaviors of Ag nanoparticles: a molecular dynamics study. *Nanotechnology* **2017**, *28*.

(156) Alarifi, H. A.; Atis, M.; Ozdogan, C.; Hu, A.; Yavuz, M.; Zhou, Y. Determination of Complete Melting and Surface Premelting Points of Silver Nanoparticles by Molecular Dynamics Simulation. *Journal of Physical Chemistry C* **2013**, *117*, 12289–12298.

(157) Alarifi, H. A.; Atis, M.; Ozdogan, C.; Hu, A.; Yavuz, M.; Zhou, Y. Molecular Dynamics Simulation of Sintering and Surface Premelting of Silver Nanoparticles. *Materials Transactions* **2013**, *54*, 884–889.

(158) Al-Rawi, A. N.; Kara, A.; Rahman, T. S. Anharmonic effects on Ag(111): a molecular dynamics study. *Surface Science* **2000**, *446*, 17–30.

(159) Kahle, L.; Musaelian, A.; Marzari, N.; Kozinsky, B. Unsupervised landmark analysis for jump detection in molecular dynamics simulations. *Physical Review Materials* **2019**, *3*, 055404.

(160) Li, M.; Han, Y.; Thiel, P. A.; Evans, J. W. Formation of complex wedding-cake morphologies during homoepitaxial film growth of Ag on Ag(111): atomistic, step-dynamics, and continuum modeling. *Journal of Physics-Condensed Matter* **2009**, *21*.

(161) Yu, J. G.; Amar, J. G. Short-range attraction, surface currents, and mound formation in metal (111) epitaxial growth. *Physical Review B* **2004**, *69*.

(162) Larsson, M. I.; Sabiryanov, R. F.; Cho, K.; Clemens, B. M. Nanopatterning of periodically strained surfaces: Predictive kinetic Monte Carlo simulation study. *Journal of Applied Physics* **2003**, *94*, 3470–3484.

(163) Li, Y. G.; DePristo, A. E. Predicted growth mode for metal homoepitaxy on the fcc(111) surface. *Surface Science* **1996**, *351*, 189–199.

(164) Schwoebel, R. L.; Shipsey, E. J. Step motion on crystal surfaces. *Journal of Applied Physics* **1966**, *37*, 3682+.

(165) Ehrlich, G.; Hudda, F. G. Atomic view of surface self-diffusion - tungsten on tungsten. *Journal of Chemical Physics* **1966**, *44*, 1039–&.

(166) Morgenstern, K.; Rosenfeld, G.; Laegsgaard, E.; Besenbacher, F.; Comsa, G. Measurement of energies controlling ripening and annealing on metal surfaces. *Physical Review Letters* **1998**, *80*, 556–559.

(167) Shen, M.; Jenks, C. J.; Evans, J. W.; Thiel, P. A. Rapid decay of vacancy islands at step edges on Ag(111): step orientation dependence. *Journal of Physics-Condensed Matter* **2010**, *22*.

(168) Giesen, M.; Ibach, H. On the mechanism of rapid mound decay. *Surface Science* **2000**, *464*, L697–L702.

(169) Towns, J.; Cockerill, T.; Dahan, M.; Foster, I.; Gaither, K.; Grimshaw, A.; Hazlewood, V.; Lathrop, S.; Lifka, D.; Peterson, G. D.; et al., XSEDE: Accelerating Scientific Discovery. *Computing in Science & Engineering* **2014**, *16*, 62–74.